Surface electronic bands of submonolayer Ge on Ag(111)

E. Golias, E. Xenogiannopoulou, D. Tsoutsou, P. Tsipas, S. A. Giamini, and A. Dimoulas*

National Center for Scientific Research DEMOKRITOS, Patriarchou Grigoriou and Neapoleos, 15310, Aghia Paraskevi, Athens, Greece

(Received 4 February 2013; revised manuscript received 27 June 2013; published 5 August 2013)

Germanium deposited on single-crystal Ag(111) substrates at about 1/3-monolayer coverage forms a stable $(\sqrt{3}\times\sqrt{3})R30^\circ$ superstructure as seen by reflection high-energy electron diffraction. *In situ* angle resolved photoelectron spectroscopy reveals a rich band structure consisting of conelike features that cross the Fermi surface at the center ($\bar{\Gamma}$ points) of the superstructure surface Brillouin zone (SBZ), exhibiting a high dispersion with the surface parallel wave vector. With the help of first-principles calculations, it can be inferred that most of the features are explained in terms of an Ag_2Ge-ordered surface alloy corresponding to surface states localized in the first two layers. One of the bands has a saddle point near the $\bar{M}$ point of the SBZ with a characteristic split-band behavior distinguishing Ge surface alloy from other similar systems.

DOI: 10.1103/PhysRevB.88.075403 PACS number(s): 73.20.At, 73.22.−f, 79.60.−i

I. INTRODUCTION

Surfaces are physical systems where inversion symmetry is broken, allowing the lift of spin degeneracy of the electronic states. At metal surfaces, the broken spatial symmetry provokes a split of the degenerate electronic surface states due to a mechanism known as Rashba-Bychkov (RB) effect.[1] Although the RB effect manifests itself in the surfaces of clean metals, ordered surface alloying can enhance the RB type splitting by introducing in-plane potential gradients[2] leading to novel two-dimensional (2D) electronic structures with potential applications to spintronics. The Ag(111) surface is a suitable template for a group of surface alloys with remarkable 2D electronic profiles. In particular, when 1/3 monolayer (ML) of Bi,[2] Pb,[3] Sb,[4] or Sn[5] are deposited on Ag(111), the $(\sqrt{3}\times\sqrt{3})R30^\circ$ superstructure is formed by substituting one out of three Ag surface atoms. The RB split ranges from the giant splitting of Bi/Ag(111) down to the untraceable split of Sn/Ag(111).

Additionally, the Ag(111) surface is presently the material of choice for growing 2D graphenelike phases of Si, known as silicene.[6] Unlike the above-mentioned metal atoms, Si does not react with silver atoms but rather wets the Ag(111) surface and forms various 2D honeycomb lattices.[7] On the other hand, the Ge counterpart of silicene, namely germanene, has been predicted to be stable[8] but has never been realized experimentally. Given the chemical similarity between the two semiconducting materials, Ag(111) is regarded as a suitable candidate substrate for germanene growth. Nevertheless, early attempts[9] to grow submonolayer Ge on Ag(111) revealed a $(\sqrt{3}\times\sqrt{3})R30^\circ$ superstructure attributed to the Ag_2Ge-ordered surface alloy similar to the group of surface alloys with RB-type spin-split states. Apart from a generic ultraviolet photoelectron spectroscopy study of valence-band states,[9] a systematic mapping of the band structure of the Ge/Ag(111) surface alloy using angle-resolved photoemission spectroscopy (ARPES) is currently missing. The Ge surface alloy complements the previously reported cases of Bi, Pb, Sb, and Sn. The trend is that RB-type split states weakens with decreasing atomic number in the $(\sqrt{3}\times\sqrt{3})R30^\circ$ Ag(111) surface alloy family; however, a detailed mapping is important since the RB split states can be realized on systems without heavy elements, as for example, in the case of Br/Ge(111).[10]

In this work we present a complete imaging of the electronic profile of the Ge/Ag(111) system using *in situ* angle-resolved photoelectron spectroscopy (ARPES). The band structure of the Ge surface alloy shows similar characteristics with the previously reported surface alloys on Ag(111), the most noticeable of which are 2D highly dispersing bands crossing the Fermi surface at the zone center of the superstructure surface Brillouin zone (SBZ). Assuming a substitutional Ag_2Ge-ordered surface alloy, first-principles calculations in the density functional theory (DFT) framework were performed in order to correlate the observed band structure with the calculated electronic features of a slab model with 1/3 ML of Ge on Ag(111), predicting most, but not all, of the experimental findings.

This article is organized as follows. In Sec. II the growth along with the structural and chemical characterization of the prepared sample are reported. Section III presents a detailed mapping of the superstructure's electronic profile using ARPES. First-principles calculations and a correlation with the experimental results are presented in Sec. IV. Finally, in the discussion and conclusions sections, an interpretation of the experimental and theoretical data is considered.

II. GERMANIUM GROWTH ON SILVER

The growth experiments have been performed in an ultrahigh vacuum molecular beam epitaxy system with base pressure in the high 10^{-10} Torr range, equipped with reflection high-energy electron diffraction (RHEED). Mirrorlike polished Ag(111) single crystals were commercially available with premarked in-plane $[1\bar{1}0]$ and $[\bar{1}\bar{1}2]$ crystallographic orientations, which were also verified by recording well-known diffraction patterns by RHEED. Ag substrate was cleaned in vacuum by 1.5-keV Ar ion sputtering for 30 min at 5×10^{-5} mbar. Subsequently, annealing in vacuum at 500 °C for 30 min was performed to cure Ar ion sputtering damage and obtain flat and well-ordered surfaces as monitored by streaky RHEED patterns. The annealing-sputtering cycle was repeated as many times as necessary to obtain a clean surface free of C and O contaminants as verified by *in situ* x-ray photoelectron spectroscopy (XPS). Perfectly clean Ag(111) showed an intense Shockley-type surface state (SSS) as seen in the Supplemental Material.[11] Ge was evaporated at room

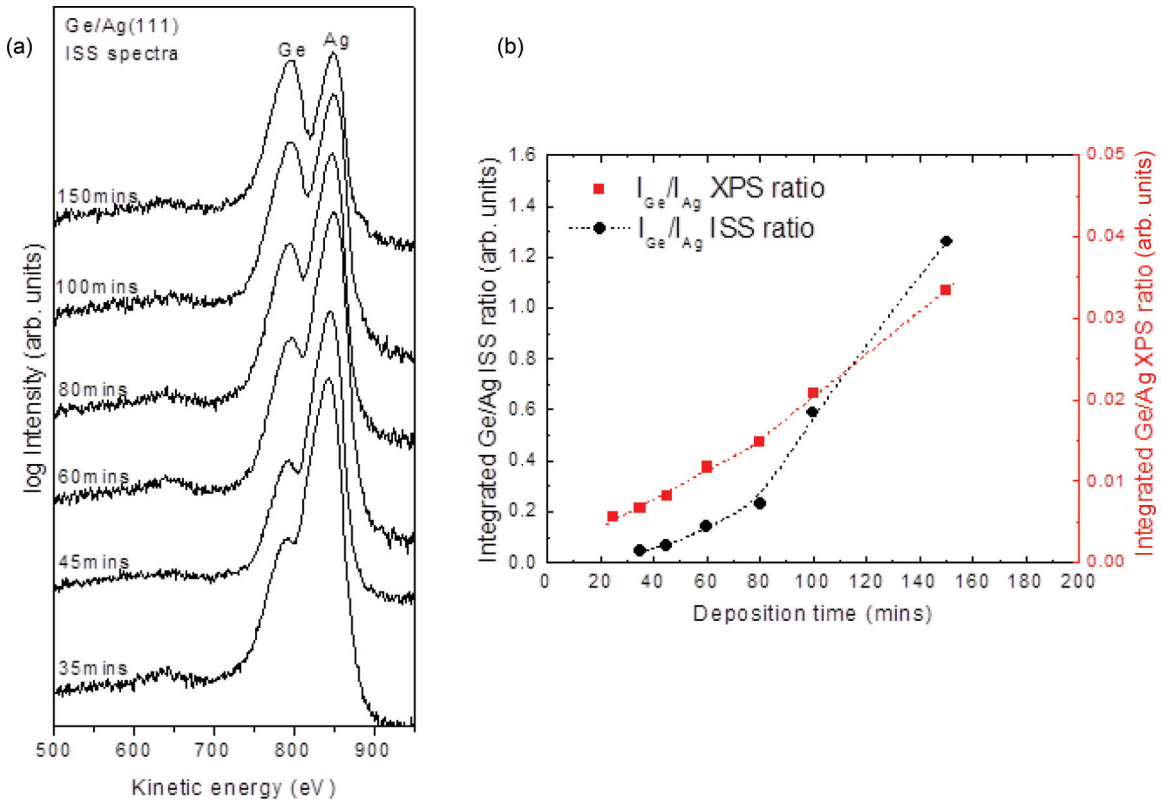

FIG. 1. (Color online) (a) He^+ LEISS spectra of Ge-deposited Ag(111) samples for various Ge deposition times, using the low deposition time rate of 0.03 Å/min. Data acquired for 1-keV incident energy. (b) Integrated Ge/Ag intensity ratio of Ge-deposited Ag(111) samples for various Ge deposition times using the low deposition time rate of 0.03 Å/min. Black circles represent He^+ LEISS data acquired for 1-keV incident energy. Dashed line is guide to the eye. Red rectangles represent XPS data acquired at 38° with respect to sample normal, using an Al source. Ge 3*d* and Ag 3*d* XPS peaks were used for the calculations. One-monolayer coverage is reached at about 80-min deposition time.

temperature on the clean Ag(111) surface from a Ta effusion cell heated at either 1040 °C or 1250 °C to produce two different evaporation rates of 0.03 Å/min and 1.4 Å/min, respectively. Both evaporation rates produced the same results. The slow rate was estimated from surface coverage data obtained by low-energy ion scattering spectroscopy (LEISS) and XPS. Figure 1(a) shows the ISS spectra of Ge-deposited Ag(111) samples for various deposition times, where the ISS peaks of Ge and Ag are observed. Increasing deposition time, the Ge peak increases with respect to the Ag peak. The variation of Ge to Ag intensity ratio from the respective ISS signals and also from XPS signals, as a function of deposition time is given in Fig. 1(b). The ML formation seems to occur around 80-min deposition time, where a change in the experimental curves slope is observed. This change is better resolved in the LEISS data, probably because the latter technique is inherently sensitive to the outermost layer compared to XPS.

At about 1/3-ML Ge coverage, which that is obtained at 30-min deposition time, the RHEED patterns in Fig. 2 show a ×3 and ×1 reconstruction along the two perpendicular $[\bar{1}\bar{1}2]$ and $[1\bar{1}0]$ azimuths, respectively. In the same Fig. 2, the simulated reciprocal space for a $(\sqrt{3} \times \sqrt{3})R30°$ surface superstructure with respect to the (1 × 1) Ag(111) is shown for comparison. The superstructure spots in the reciprocal space can be correlated with the additional faint RHEED

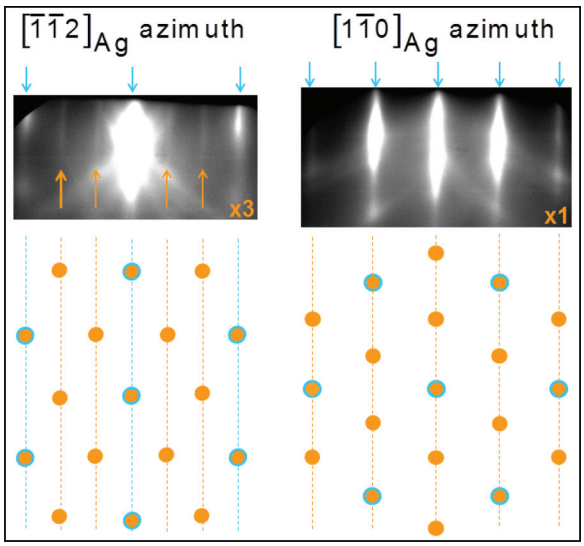

FIG. 2. (Color online) RHEED diffraction patterns of Ge/Ag(111) at 1/3-ML coverage obtained along the $[\bar{1}\bar{1}2]$ and $[1\bar{1}0]$ azimuth of Ag(111) surface. Blue and orange arrows indicate the diffraction streaks of Ag(111) and Ge/Ag(111) superstructure, respectively. Schematic below illustrates a simulated LEED image of $(\sqrt{3} \times \sqrt{3})R30°$ superstructure on Ag(111). Open blue and filled orange circles correspond to Ag(111) and $(\sqrt{3} \times \sqrt{3})R30°$ diffraction spots, respectively.

diffraction streaks observed at 1/3 and 2/3 positions when the sample is probed by the e-beam along the $[\bar{1}\bar{1}2]$ azimuth, explaining the $\times 3$ reconstruction. On the other hand, when the sample is probed along the $[1\bar{1}0]$ azimuth, the superstructure spots are aligned with the Ag diffraction spots, showing no additional streaks in RHEED. Therefore, the RHEED data are compatible with a $(\sqrt{3} \times \sqrt{3})R30^\circ$ superstructure forming on the surface in agreement with earlier report.[9] It should be noted that the RHEED patterns in Fig. 2 are preserved becoming more intense after annealing up to 140 °C. When the coverage increases away from 1/3 ML deposition, the pattern abruptly changes becoming significantly more complex so that the correlation with certain superstructure symmetry is difficult.

III. SURFACE BAND STRUCTURE IMAGING

The valence-band structure of Ge/Ag(111) at 1/3-ML Ge coverage was investigated by room-temperature *in situ* ARPES without breaking vacuum in a μ-metal analytical chamber with low 10^{-9} Torr base pressure, equipped with a 100-mm hemispherical electron analyzer and a 2D charge-coupled device detector. The energy resolution of the detection system was better than 40 meV using 21.22-eV photons from a He discharge source. Ne and Ar discharge sources with 16.67-eV and 11.62-eV photons, respectively, were also used to complement data. For each azimuth angle φ of the sample, the polar angle ϑ varied from (-12 to 65°) with step angle of 1° and tilt window of 29.5°. Measurements were made for five different azimuth angles φ covering total azimuth range $\Delta\phi = 120^\circ$.

In Fig. 3, an overview of the probed k space is given in the constant energy contour plots k_x-k_y at binding energy $E_B = -0.05$ eV near Fermi level [Fig. 3(a)] and at $E_B = -1.21$ eV [Fig. 3(b)]. While the bulk Ag sp band (B), observed in clean Ag (111) is still visible, the Ag SSS state (see Supplemental Material in Ref. 11) has disappeared and different features have developed in place after Ge deposition. In Fig. 3(a), these Ge-related features consist of inner circular (S_1, S_3) and outer snowflake (or starlike) bands (S_2) located at the center ($\bar{\Gamma}$ point) of the first SBZ and at the center of all adjacent SBZs of the superstructure. In Fig. 3(b), part of the S_2 band is still faintly visible while a very intense feature (S_4) appearing at the $\bar{\mathrm{M}}$ point of Ag (or equivalently at the $\bar{\mathrm{M}}'$ point of the superstructure SBZ) is essentially a continuation of the S_2 band showing up at larger binding energies ($E_B = -1.21$ eV). It should be noted that S_1-S_4 are all surface (2D) bands since they show no variation as a function of the excitation energy as discussed at the end of this section. The Ge-related surface bands are clearly detected when Ge is deposited at room temperature, but their ARPES intensity is markedly increased when samples are annealed up to 140 °C. In addition, the surface bands in Fig. 3(b) rapidly lose their intensity when more Ge is deposited away from the 1/3-ML Ge coverage and they eventually disappear at around 1-ML Ge coverage, accompanied by a drastic change of the RHEED diffraction pattern as already mentioned above (see Sec. II).

The energy dispersion of the Ge/Ag(111) surface bands along the superstructure $\bar{\Gamma}\bar{\mathrm{M}}\bar{\Gamma}$ direction (or, equivalently, along the Ag $\bar{\Gamma}\bar{\mathrm{K}}$ direction) is shown in Fig. 4(a), and the corresponding constant energy contour plots k_x-k_y for three

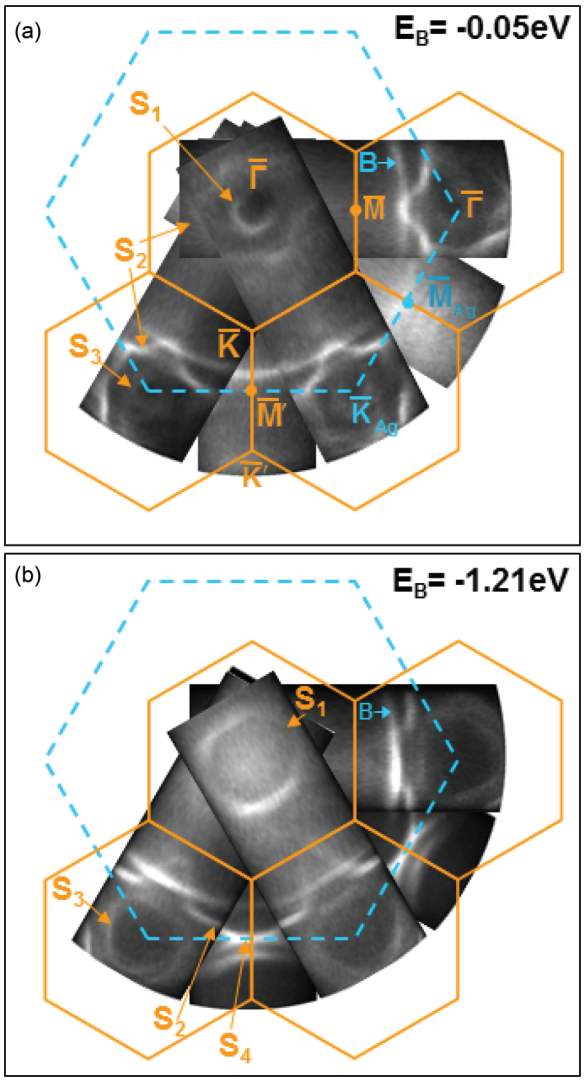

FIG. 3. (Color online) APRES constant energy contours k_x-k_y of Ge/Ag(111) superstructure probed by He I excitation at 21.22 eV: (a) near Fermi level ($E_B = -0.05$ eV) and (b) at $E_B = -1.21$ eV. (1×1) Ag(111) and $(\sqrt{3} \times \sqrt{3})R30^\circ$ superstructure SBZs are indicated by dashed blue and solid orange hexagons, respectively. High-symmetry points of the SBZ are also shown. The $\bar{\Gamma}$ points of the superstructure coincide with the $\bar{\mathrm{K}}$ points of Ag(111) SBZ. B marks the bulk Ag sp band, while S_1-S_4 are surfaces states of superstructure.

different binding energies are shown in Fig. 4(b). The bulk Ag sp band (B), observed in clean Ag(111) is still visible (see Supplemental Material in Ref. 11), but additional Ge-related highly dispersive surface bands appear, denoted by S_1, S_2, and S_3. The S_1 and S_3 bands in Fig. 4(a) vary linearly looking like part of an inner cone with apex located about 0.5 eV above E_F and with a corresponding circular projection in the $E_B = -0.2$ eV constant energy plot in Fig. 4(b). The S_2 band in Fig. 4(a) appears as part of an outer cone with a corresponding snowflake projection due to a strong hexagonal warping as seen in the $E_B = -0.2$ eV constant energy plot in Fig. 4(b). S_2 bands expand and become fader as they disperse from Fermi level to approximately ~ -1.2 eV below it. At $E_B = -1.0$ eV and higher (away from E_F), the inner cone S_1 exhibits a clear hexagonal distortion [Fig. 4(b)].

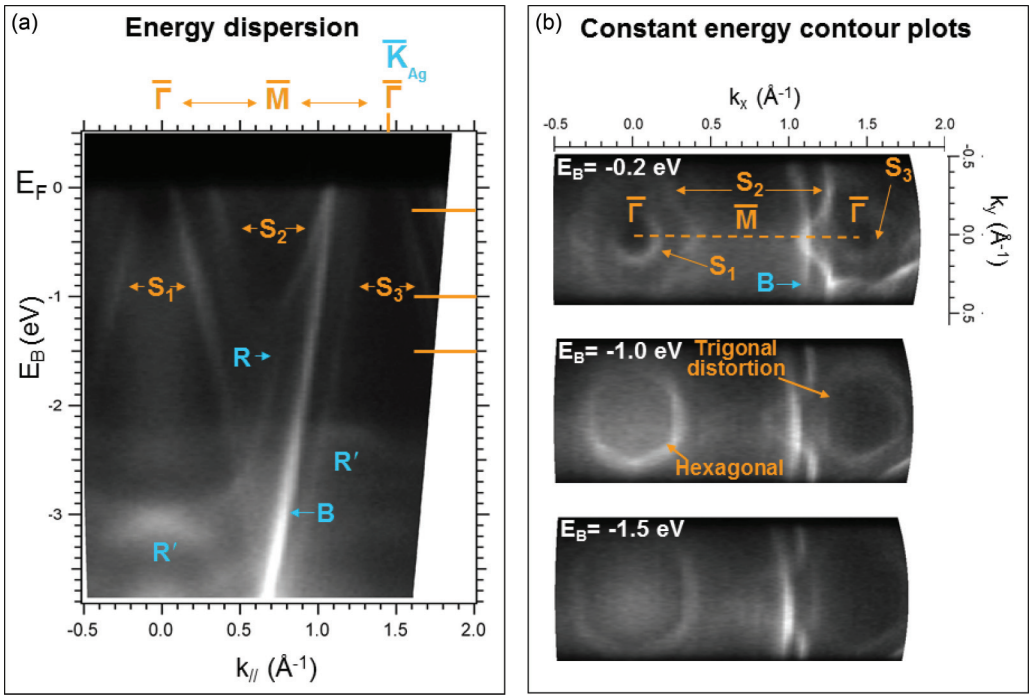

FIG. 4. (Color online) Surface electronic band structure imaging of Ge/Ag(111) along the $\bar{\Gamma}\bar{K}$ direction of the Ag(111) SBZ (or $\bar{\Gamma}\bar{M}\bar{\Gamma}$ direction of the superstructure SBZ) using ARPES with He I excitation at 21.22 eV. (a) Energy vs k_x dispersion for $k_y = 0$. B and R denote the bulk Ag *sp* band and its replica due to He $I_{\beta\gamma}$ excitation at 23.09 eV, respectively. R' denotes the replicas of Ag *d* bands. The horizontal orange lines mark the binding energies E_B at which the constant energy contours k_x-k_y are plotted in (b). S_1, S_2, and S_3 mark highly dispersive surface bands appearing as a result of Ge deposition on Ag.

The energy dispersion of the Ge/Ag(111) surface bands along the superstructure $\bar{\Gamma}$-$\bar{K}$-$\bar{M}'$ direction (or, equivalently, along the Ag $\bar{\Gamma}\bar{M}$ direction) is shown in Fig. 5(a), and the corresponding constant energy contour plots k_x-k_y for three different binding energies are shown in Fig. 5(b). The inner conelike (S_1) and outer warped cone or snowflake (S_2) features at $\bar{\Gamma}$ are clearly visible in both Figs. 5(a) and 5(b) as well as the hexagonal distortion of the inner cone S_1 at E_B higher than -1.0 eV [Fig. 5(b)]. The most notable observation is the strong intensity feature S_4 at the superstructure $\bar{M}'$ point (or, equivalently, Ag $\bar{M}$ point) peaking at $\sim$1 eV below E_F [Fig. 5(a)]. This feature is absent in clean Ag(111) and is associated with Ge-related surface bands, despite the fact that it appears near the Ag *sp* bands. S_4 in Fig. 5(a), appears as two crossing cones (or a split cone) with apex at $E_B = -1$ eV. Nevertheless, a more detailed examination of the (k_x-k_y) constant energy plots presented in Fig. 5(b) ($E_B = -1$ and -1.5 eV), shows that the center of curvature of each branch points towards opposite directions that does not support the split conelike shape assumption. Although S_4 appears as a new feature along $\bar{\Gamma}\bar{K}\bar{M}'$ (Fig. 5), as already mentioned above, the complete mapping in k space ([Fig. 3(b)], reveals that S_4 is essentially a continuation of S_2 band. While S_2 band is part of the warped cone appearing at the $\bar{\Gamma}$ point of the superstructure (or equivalently $\bar{K}$ point of Ag) at low E_B near Fermi surface, S_4 is the "tail" of the same cone appearing at high binding energy ($E_B \sim -1.2$ eV) and extending toward the $\bar{M}'$ point, which is a saddle point for the warped conelike band S_2. This saddle point is better understood with the help of Fig. 6 showing the energy dispersion along a cut at the $\bar{M}'$-point perpendicular to the superstructure $\bar{\Gamma}$-$\bar{K}$-$\bar{M}'$-$\bar{K}'$ direction, as indicated by the dashed white line in the inset schematic of Fig. 6. The S_2 band exhibits an upward paraboliclike dispersion with a minimum at around -1.2 to -1.4 eV below the Fermi level, and energy at a reverse downwards dispersion of S_4 along the $\bar{\Gamma}$-$\bar{K}$-$\bar{M}'$-$\bar{K}'$ begins, as depicted in Fig. 5(a). This behavior indicates that S_2 and S_4 are two parts of the same band touching each other at the saddle point at $\bar{M}'$. In the k_x-k_y plots of Fig. 5(b), the scope is to show the band splitting of S_4 just below ($E_B = -1.5$ eV) and just above ($E_B = -1.0$ eV) the saddle point at $\bar{M}'$. On the other hand, in Fig. 7, the aim is to show the split-band behavior of S_2 and illustrate the connection between S_2 and S_4 with as much detail as possible. As seen in Fig. 7(a), the splitting can be resolved in that part of S_2 which is on either side of the $\bar{M}'$ point essentially replicating the behavior of S_4 at $\bar{M}'$. At higher binding energies and as the saddle point is approached [Fig. 7(b)], the two parts of S_2 join each other at the $\bar{M}'$ point forming the band that we have denoted as S_4.

The dispersion characteristics of the Ge-related features were investigated by ARPES using different excitation energies $h\nu$.[12] Figure 8 shows the k_x-k_y constant energy plots of Ge/Ag(111) measured by 21.22-eV, 16.67-eV, and 11.62-eV photon energies of He I, Ne I, and Ar I discharge sources, respectively. The only changing feature with $h\nu$ is the bulk *sp* band (B) of Ag(111) (blue lines), while conelike (S_1, S_3) and snowflake (S_2) features around the $\bar{\Gamma}$ points of $(\sqrt{3} \times \sqrt{3})R30^\circ$ superstructure do not change. The same is true for feature S_4 (data not shown here). A bulk-emission band in general dispersing with both parallel and perpendicular

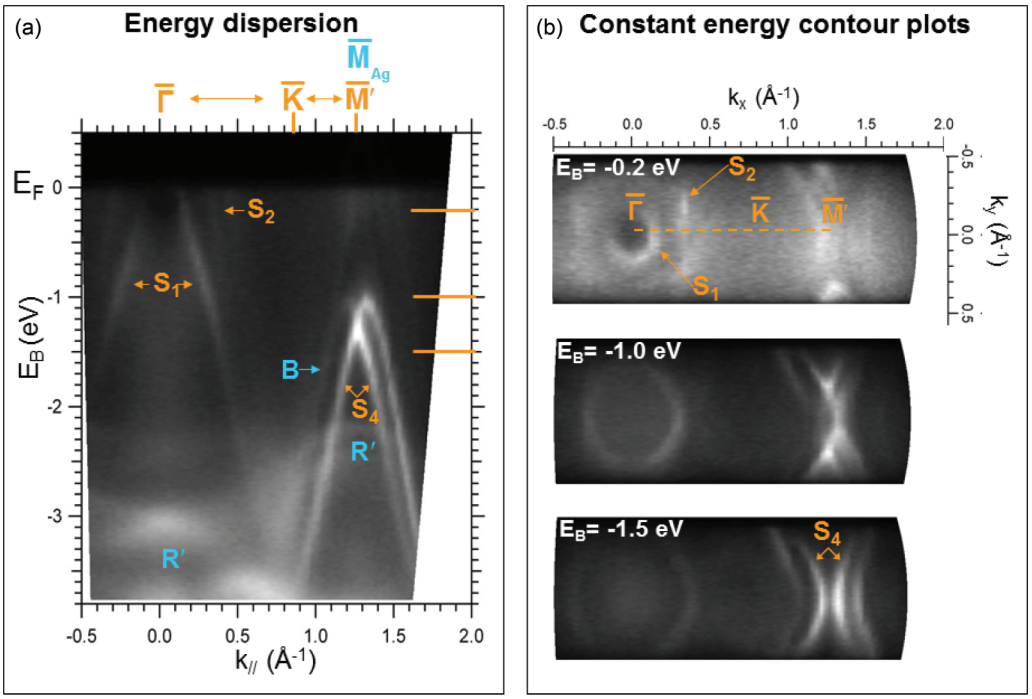

FIG. 5. (Color online) Surface electronic band structure imaging of Ge/Ag(111) along the $\bar{\Gamma}\bar{M}$ direction of the Ag(111) SBZ (or $\bar{\Gamma}\bar{K}\bar{M}'$ direction of the superstructure SBZ) using ARPES with He I excitation at 21.22 eV. (a) Energy vs k_x for $k_y = 0$. B denotes the bulk Ag *sp* band, while R′ denotes the replicas of Ag *d* bands due to He I$_{\beta\gamma}$ excitation at 23.09 eV. The horizontal orange lines mark the binding energies E_B at which the constant energy contours k_x-k_y are plotted in (b). S_1, S_2, and S_4 mark highly dispersive surface bands appearing as a result of Ge deposition on Ag.

wave vector components $k_\parallel$ and $k_\perp$, respectively, is expected to vary with changing $h\nu$ due to the dependence of $k_\perp$ on $h\nu$. In contrast, a surface band (or 2D band) disperses only with the wave vector $k_\parallel$ parallel to the surface and has no dependence on the perpendicular wave vector component $k_\perp$; therefore, it is expected to remain invariant under $h\nu$ changes. Therefore, according to the data of Fig. 8, the Ge-related S_1-S_4 features are 2D (surface) states, although it cannot be judged merely from Fig. 8 data whether they are *true* surface states or rather *resonant* surface states related to bulk Ag.

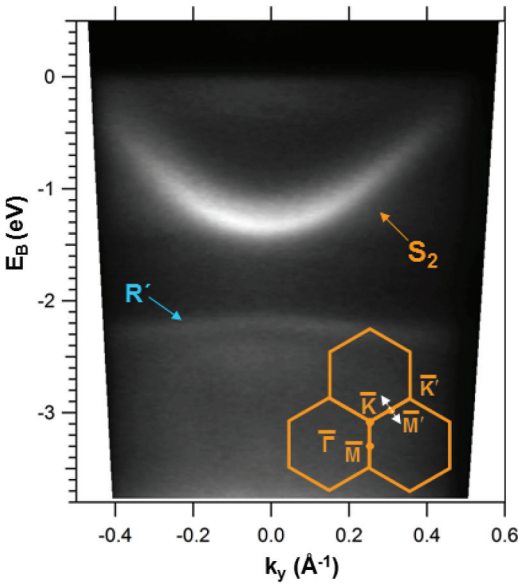

FIG. 6. (Color online) Energy dispersion of Ge/Ag(111) using ARPES with He I excitation at 21.22 eV at the saddle point of S_2 surface band. Data show the energy vs k_y for $k_x = 1.25$ Å^{-1} cut, along the direction shown by the white dashed line in the inset, where the SBZ of superstructure is shown. R indicate Ag *d* bands replicas.

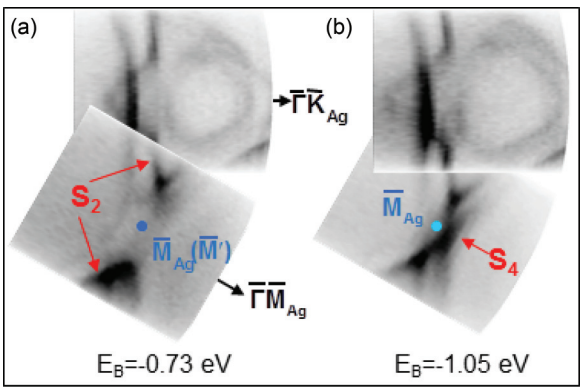

FIG. 7. (Color online) Constant energy contours of Ge/Ag(111) surface obtained at various binding energies, (a) −0.64 eV, (b) −0.85 eV, (c) −1.05 eV, and (d) −1.21 eV. The blue dot indicates the $\bar{M}_{Ag}$ point (or equivalently $\bar{M}'$ point of the superstructure SBZ) at $k_\parallel = 1.25$ Å^{-1}. In (a) the two parts of the S_2 band at the vicinity of $\bar{M}_{Ag}$ exhibit a split-band behavior. In (b) the two parts of the S_2 band merge at $\bar{M}_{Ag}$, resulting in the strong photoemission signal denoted as S_4.

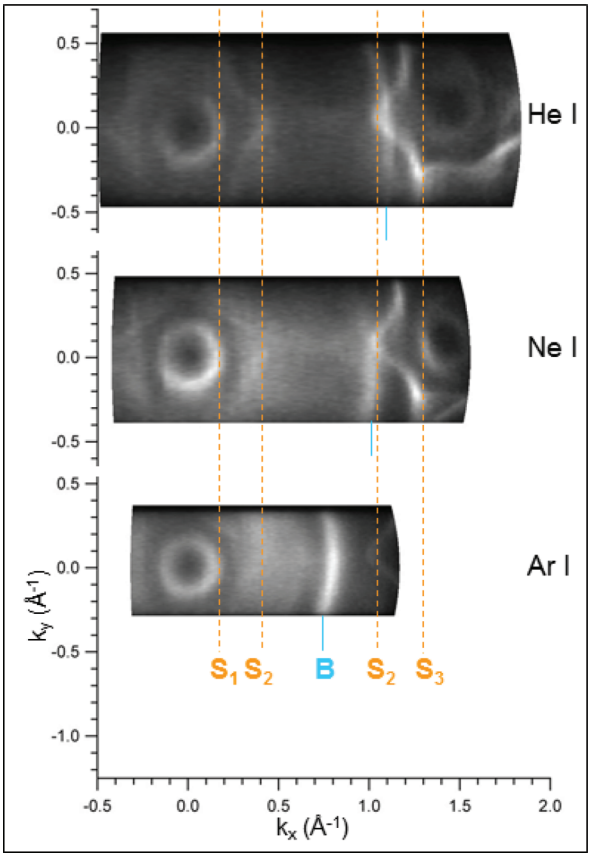

FIG. 8. (Color online) k_x-k_y constant energy plots ($E_B = -0.3$ eV) of Ge/Ag(111) surface acquired by ARPES with different excitation energies $h\nu$: He I 21.22 eV, Ne I 16.67 eV, and Ar I 11.62 eV. Measurements are along Ag(111) $\bar{\Gamma}\bar{\mathrm{K}}$ direction of BZ. Unchanged surface bands (S_1, S_2, S_3) are marked by orange lines, while changing bulk Ag bands (B) are indicated by blue lines.

IV. FIRST-PRINCIPLES CALCULATIONS

The most plausible atom arrangement in real space compatible with a $(\sqrt{3}\times\sqrt{3})R30^\circ$ superstructure is the substitutional Ag_2Ge-ordered surface alloy as first proposed for the Ge/Ag(111) system[9] and for the similar systems Pb/Ag(111),[3] Bi/Ag(111),[2] Sb/Ag(111),[4] and Sn/Ag(111).[5] To simulate the Ag_2Ge surface alloy, we have used a ten layer slab in the supercell geometry, based on the calculated lattice constant of bulk Ag ($a = 4.15$ Å). One out of three Ag atoms at one surface of the slab was substituted by a Ge atom to reproduce the $(\sqrt{3}\times\sqrt{3})R30^\circ$ surface alloy. More than 18 Å of vacuum was included to ensure the isolation of the two sides of the slab. The calculations were performed within the DFT framework using the Vienna *Ab initio* Simulation Package[13] code. We used a general gradient approximation[14] exchange-correlation functional, and projector-augmented wave potential.[15] A plane-wave basis was used up to the cutoff energy of 325 eV and a $11\times11\times1$ Monkhorst-Pack grid was employed for sampling the reciprocal space. All the atoms, with the exception of the two bottom layers, were allowed to relax until the force and the energy were converged to 10^{-2} eV/Å and 10^{-4} eV, respectively. The results of relaxation are depicted in Fig. 9. The Ge atoms take stable positions only 0.09 Å below the surface essentially lined up with the Ag top surface atoms. This may partly explain the fact that it was not possible to visualize Ge atoms in early STM experiments.[9]

The resulted charge density was used to calculate the electronic band structure, along high-symmetry directions in k space as shown in Fig. 10(a). The symbols represent the wave-function character around the Ge surface atom. The size of the symbols is proportional to the overlap of the surface alloy bands with orbitals around the Ge atom. The experimental band dispersion curves are also drawn with thick solid lines on the same Fig. 10(a) for a direct comparison with the DFT results. In Fig. 10(a), the calculations do not include spin-orbit interaction in the valence orbitals. Note however, that additional calculations (not shown here) taking the spin-orbit interaction into account in the scalar relativistic approximation did not produce significant deviations apart from a small splitting at large binding energies > -3 eV. Three upwards dispersing parabolic features around the zone center (mainly of s, p_z character) can be associated with quantum well states due to the finite slab thickness used in the calculation. These quantum well states have been previously observed in surface alloys grown in a confined geometry;[16,17] however, in bulk Ag as in our case here, the quantum well states are expected to merge in a continuum of states resulting only in a featureless background in agreement with our observations in Figs. 4(a) and 5(a). The downwards dispersive branches, starting at 1.2 eV above the Fermi level, show asymmetric behavior towards $\bar{\Gamma}\bar{\mathrm{K}}$ and $\bar{\Gamma}\bar{\mathrm{M}}$ paths. Both branches are made of orbitals lying in the x-y surface plane; the branch along the $\bar{\Gamma}\bar{\mathrm{M}}$ direction has a pure p_x character, while the one along the $\bar{\Gamma}\bar{\mathrm{K}}$ is a mixture of p_x and p_y orbitals. Additionally, a reverse broken parabolic feature with its maximum at $E_B = -0.47$ eV is a mixture of s and p orbitals. The minigaps along the parabola may be attributed to the hybridization of the surface bands with the aforementioned quantum well states.[16,17] Along the path of the Brillouin zone boundaries ($\bar{\mathrm{K}}\bar{\mathrm{K}}'$), the dispersive feature with a maximum at $E_B = -1$ eV has a p_x character.

By a simple inspection of Fig. 10(a), it can be inferred that there is a very good agreement between theory (symbols) and experiment (red solid lines) for the outer S_2 snowflake band at $\bar{\Gamma}$. Theory also describes quite well the band dispersion S_4 around the superstructure $\bar{\mathrm{M}}'$ point, although it does not reproduce the splitting observed in Figs. 5(a) and 10(a). In contrast, theory cannot explain satisfactorily, the linear variation of the inner S_1 cone near the Fermi surface.

In Fig. 10(b) a scatter plot of the orbitals around the Ge surface atom is presented at the constant energy of $E_B = -0.07$ eV near E_F. Contributions from energy levels within 50 meV around the above-mentioned value are included to create the constant energy plot. The experimental data derived from the constant energy contour plots are drawn by thick solid lines for comparison. The striking agreement between theory and experiment for the snowflake feature indicates that p_x, p_y Ge orbitals of the Ag_2Ge alloy could be responsible for this feature observed in Figs. 4(b) and 5(b). The same Ge orbitals describe well the snowflake feature for smaller binding energies too (not shown here). In contrast, there are no Ge or Ag orbitals near the experimental circular projection of the inner cone (solid circle), indicating that theory

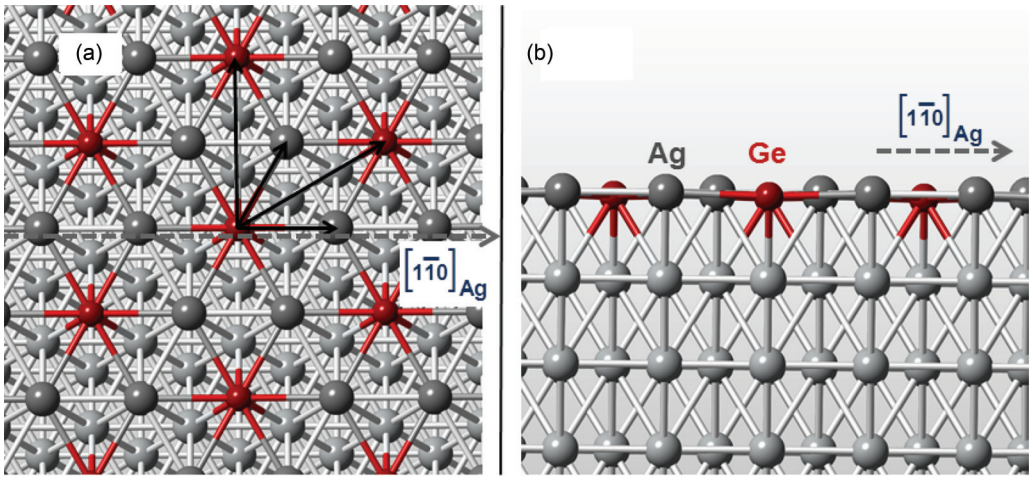

FIG. 9. (Color online) Atom configuration of the DFT optimized Ge $(\sqrt{3} \times \sqrt{3})R30^\circ$ superstructure. Red and gray spheres represent Ge and Ag atoms, respectively. Dark gray spheres represent top surface Ag atoms. (a) Top view showing 2D basis vectors of the Ag(111) surface (long vectors) and the superstructure (short vectors). (b) Side view along the $[1\bar{1}0]$ Ag direction. Ge atoms relax 0.09 Å below the plane defined by the top surface Ag atoms.

fails to explain the behavior of the inner conelike feature near E_F, as already argued in the description of Fig. 10(a) above.

It should be noted that the orbitals around the Ag atoms near the surface, as shown in Fig. 11, have identical dispersion and positioning as the Ge orbitals, while their total contribution is smaller compared to the Ge atoms. The s, p-type orbitals and the in plane d-orbitals, d_{xy} and $d_{x^2-y^2}$ have significant contribution to the observed features in the BE range above -3 eV. More specifically, the inner conelike shape has an s,$d_{x^2-y^2}$ character around the Ag surface atoms. The snowflakelike band is a mixture of p_x,d_{xy} along the $\bar{\Gamma}\bar{M}$ high-symmetry direction and is composed of s, p_x, p_y, and d_{xy} orbitals along the $\bar{\Gamma}\bar{K}$ direction. Finally, the S_4 feature at the $\bar{M}$ point of the superstructure is a combination of s and p_x orbitals. The S_1, S_2, S_3, and S_4 features are located at the top two layers of the superstructure. Our model calculations show that all these alloy-related features decay rapidly with depth and they are completely vanished when we reach the third layer of the structure (Fig. 11). The predicted rapid decay of the S_1-S_4 states in combination with their excitation energy invariance as shown in Fig. 8, indicate that they are surface

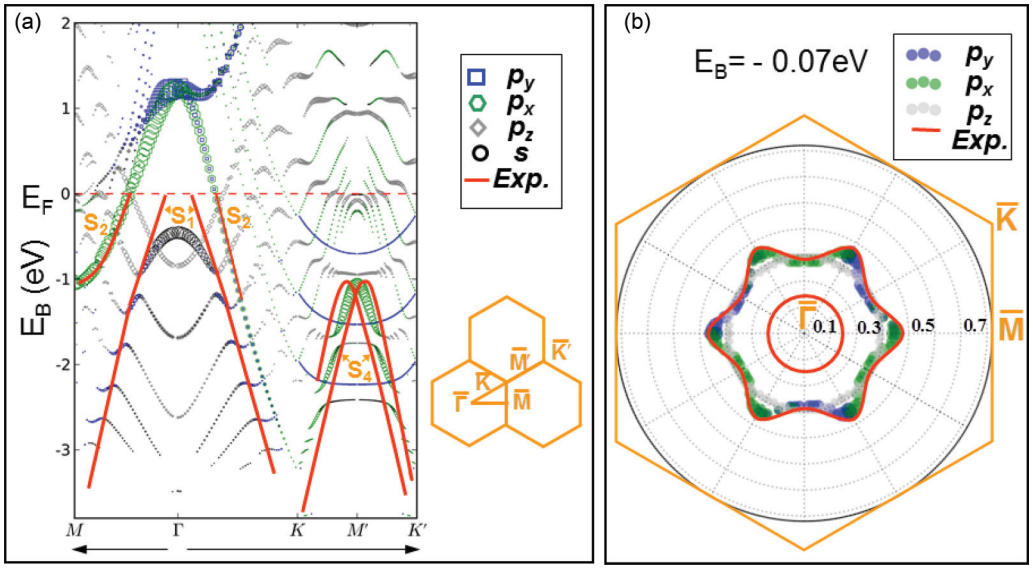

FIG. 10. (Color online) DFT band structure calculations (symbols) and experimental data (red solid lines) shown on the same plot for comparison. The symbols represent the projection of the Ge/Ag(111) alloy bands onto the atomic orbitals around the surface Ge atom. The size of the symbols is proportional to the magnitude of the overlap. (a) Band dispersion along the high-symmetry lines of the SBZ. The schematic shows the path along high-symmetry points in k space where the band structure is calculated. (b) Constant energy polar plot of the Ge atomic orbitals near E_F ($E_B = -0.07$ eV). Blue, green, and gray spots correspond to p_y, p_x, and p_z orbitals, respectively. The orange hexagon indicates the first Brillouin zone of the superstructure.

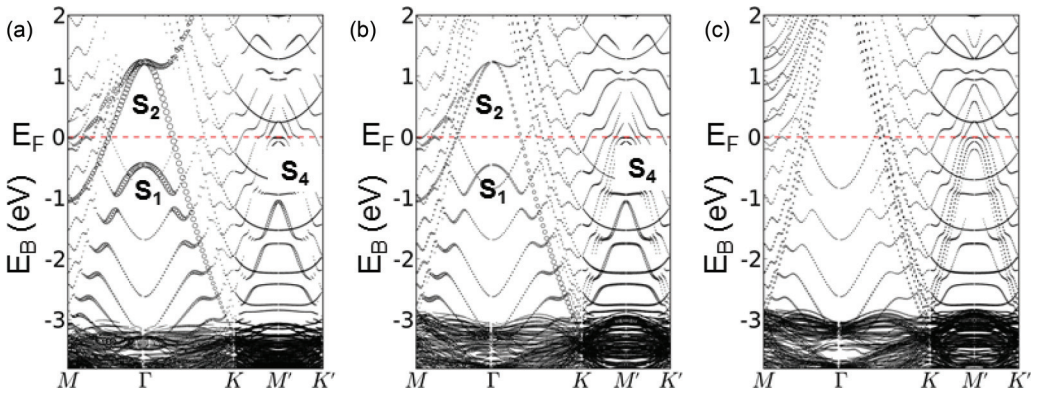

FIG. 11. Sum of all projections of the surface alloy bands on the Ag atom in the (a) $(\sqrt{3}\times\sqrt{3})R30^\circ$ superstructure surface (b) Subsurface layer and (c) two layers below the superstructure, where surface states contributions S_1, S_2, and S_4 become obsolete. The size of the black circles is proportional to the magnitude of the overlap between the surface alloy bands and the sum of all orbitals centered at Ag atoms.

states, resulting from the hybridization of Ge and Ag orbitals localized near the topmost surface layers.

V. DISSCUSSION

It is not straightforward to interpret the double-cone structure (inner S_1 and outer S_2 cone) as seen in Fig. 5(a). A possible scenario is that we observe part of two overlapping spin-polarized parabolic bands that are split in k space due to large RB effect. This is similar to what has been previously reported for the Pb/Ag(111)[3] and Bi/Ag(111)[2] systems with the same $(\sqrt{3}\times\sqrt{3})R30^\circ$ superstructure. However, the consensus is that Rashba splitting in the latter two systems occurs because there is a large atomic scale surface corrugation due to the sizable displacement of Pb and Bi atoms 0.46 and 0.65 Å, respectively, above the Ag surface atoms.[18] In contrast, Ge is predicted to be almost at the same level [see Fig. 9(b)] as the Ag top layer, so in the absence of a corrugation, no Rashba splitting is expected. Indeed, an attempt to fit the double cone S_1-S_2 structure by a set of two Rashba-type parabolic bands $E(\vec{k}) = \frac{\hbar^2}{2m^*}(|\vec{k}| \pm k_o)^2 + E_o$,[19] where E_o is the band maximum and $k_0 = \frac{\alpha_R m^*}{\hbar^2}$ is the momentum offset (α_R and m^* are the Rashba parameter and effective mass, respectively), gives very poor results; the main reason being that the inner conelike feature has clearly a linear dispersion near E_F. In addition, the outer conelike feature S_2 is satisfactorily described by DFT (Fig. 10) assuming substitutional Ag_2Ge-ordered surface alloy with no spin-orbit coupling (SOC) at all, implying that spin-orbit interaction plays no essential role in the formation of the double-cone structure through Rashba splitting.

It should be noted at this point that the experimental results for the Ge/Ag(111) system are similar to the results obtained recently on Sn /Ag(111) system,[5] where it is also mentioned that RB effect plays no role in the observed electronic band structure.[5] One important difference is that band S_4 appears to be spit in two branches (Fig. 5), while the corresponding band in Ref. 5 appears to be degenerate. As already discussed in Sec. III [Fig. 3(b)], S_4 is connected to the snowflake band S_2 at the $\bar{K}$ point of Ag, and the splitting is also observed in the part of the S_2 warped cone, which is located closer to the $\bar{M}$ point, although not so easily detectable due to limited resolution. The origin of the S_4 spitting, which is not predicted by DFT (Fig. 10), is not clear. Coexisting of two Ag_2Ge surface alloy configurations with different lattice parameters and therefore different k space could be a plausible explanation, which, however, is not supported by the RHEED data that show a clear $(\sqrt{3}\times\sqrt{3})R30^\circ$ pattern with no additional diffraction streaks. Furthermore, from the splitting in Fig. 5(a), the difference $\delta k_{\bar{M}}/k_{\bar{M}}$ in the position of $\bar{M}$ in k space is estimated to be about 11% implying a corresponding 11% difference for the lattice constant of the Ag_2Ge superstructure, which is very high and not easily explainable in terms of structural changes as for example due to strain effects or other surface step defects. Moreover, it is reasonable to expect that a lattice parameter variation would affect the band structure not only near $\bar{M}$ but also in other points of the SBZ as for example around and near the $\bar{K}$ point of Ag inducing a similar splitting in the S_2 snowflake band. However, a large part of this band (e.g., the tip of S_2 along Ag $\bar{\Gamma}\bar{K}$) shows no evidence of appreciable splitting. All of the above suggest that structural modulations could be excluded as possible origin of the split band behavior.

An alternative scenario could be based on the raising of spin degeneracy and the formation of two spin-polarized bands, relating to unconventional Rashba effect. For example, a peculiar spin splitting has been reported in a β-Bi/Si(111)-$(\sqrt{3}\times\sqrt{3})$ system[20,21] yielding nonvortical spin-split bands at the $\bar{M}$ point, notably similar to the ones obtained here in this paper. The origin of this splitting is attributed either to 2D surface symmetry[20] or to Bi trimer formation,[21] while the intrinsic SOC is considered[21] to play a less important role, implying that systems with weak intrinsic SOC like Ge/Ag(111) may exhibit similar spin splitting effects. In any case, a proof of a spin splitting effect would require additional spin-resolved ARPES experiments.

A third explanation can be formulated by making the analogy with the observations for the similar Sn/Ag(111) system.[5] In the latter system, a dispersive feature (DF) has been observed around the $\bar{M}$ point dispersing at lower binding energies near E_F. It is possible that a similar DF feature is also present in our Ge/Ag(111) system, albeit dispersing at a higher binding energy near $E_B = -1$ eV, thus hybridizing with the S_4 band, in which case two lobes could be formed appearing as a split in Fig 5(a). The origin of the DF is not known and, exactly like in Ref. 5, this feature is not predicted by first-principles

calculations, thus complicating interpretation of experimental observations.

The limited success of first-principles calculations (DFT) to accurately predict the crossing of S_1 cone at the Fermi level and the splitting of S_4 band at the $\bar{\mathrm{M}}$ point, calls for a careful consideration of the structural model used here, namely, the ordered Ag_2Ge substitutional surface alloy. Within this model and by making only a small modification in the Ge position, the situation is markedly improved. More specifically, if the Ge atom is raised and kept fixed above the surface by about 0.5 Å from the Ag surface atoms (or ∼0.6 Å from its most stable position), then the S_1 band crosses the Fermi surface near $\bar{\Gamma}$ (see Supplemental Material in Ref. 11) better conforming with the experimental observation albeit with a small offset in the k values, where S_1 crosses E_F and a small deviation in the energy position of the S_2 band. This could bridge the discrepancies between theory and experiment provided that one can accept that Ge could be located in a less stable configuration as predicted by DFT.

Then, we consider possible deviations from surface coverage that could significantly modify the structural surface configuration away from the substitutional Ag_2Ge model. As already mentioned in Sec. II, LEISS and XPS (Fig. 1) indicate that 1-ML coverage is achieved approximately after 80-min deposition. The Ge deposition time is about 30 min until a clear $(\sqrt{3}\times\sqrt{3})R30^\circ$ is obtained, meaning that we are near the 1/3 Ge coverage condition in compatibility with the Ag_2Ge stoichiometry. Nevertheless, a small deviation from this coverage and stoichiometry cannot be excluded. A uniform coverage of about 2/3 Ge could be consistent with Ge adatoms forming Ge-Ge dimers with the same superstructure. A DFT calculation of this configuration improves the S_1 dispersion near E_F but totally misses the S_2. Finally, 1 ML coverage with Ge atoms sitting on top, bridge, or hollow positions over the Ag(111) lattice results in a band structure having no resemblance with the experimental one in Figs. 4 and 5.

An alternative configuration that deserves special attention is germanene, a honeycomb lattice formed by placing Ge atoms in the hollow positions of Ag surface atoms, which is also compatible with the $(\sqrt{3}\times\sqrt{3})R30^\circ$ superstructure observed by RHEED (Fig. 2). Assuming such a Ge honeycomb lattice, a possible scenario is that, here, we witness the π bands of a graphenelike surface structure crossing at about 0.5 eV above the Fermi level. If that would be the case, the Fermi velocity derived from the slope of S_1 curves would be 0.85×10^6 m/s, compatible with predicted values for germanene.[8] However, the Dirac cone of a graphenelike structure, including free-standing germanene, is normally expected at the edge ($\bar{\mathrm{K}}$ points) of the superstructure SBZ rather than at the center ($\bar{\Gamma}$ point). In our case, the observation of a possible Dirac cone at the center of the SBZ could be a signature of strong modification of germanene electronic band structure due to the influence of the substrate or a modification as a result of the predicted nontrivial topological order[22] in germanene. It should be noted however, that the assumption of germanene coexistence with the Ag_2Ge surface alloy finds little support from DFT band structure calculations. In addition, the Ge honeycomb lattice considered here is highly strained (tensily) at about 19%. Although small 2D clusters of strained germanene with only a small amount of build-up elastic energy could be stable, this value of strain is still unrealistically high; therefore, the assumption of germanene formation (in coexistence with Ag_2Ge alloy) is dubious.

VI. SUMMARY AND CONCLUSIONS

The decoration of Ag(111) surface with Ge atoms at around 1/3-ML coverage results in a $(\sqrt{3}\times\sqrt{3})R30^\circ$ superstructure and a rich and highly dispersive 2D metallic surface band that is dominated by a double-cone structure crossing the Fermi surface at the center ($\bar{\Gamma}$ point) of the superstructure SBZ. The analysis shows that the double-cone structure may not be a result of Rashba-type splitting. Assuming a substitutional Ag_2Ge-ordered surface alloy, DFT calculations predict that in its most stable state, Ge resides very near the surface, only 0.09 Å below the top layer. Among other structural models considered, the substitutional Ag_2Ge one is the most successful in describing the experimental band structure, although it slightly misses the behavior of the inner cone near the Fermi surface. Notably, positioning Ge 0.5 Å above the surface or 0.6 Å away from its most stable position, bridges the discrepancy between theory and experiment for the inner cone. The model describes extremely well the outer warped cone band in a large portion of the k space except from the area near the $\bar{\mathrm{M}}$ point, where the band has a saddle point at about 1.2 eV below the Fermi level. This is clearly imaged by ARPES although an unexpected split band effect appears that cannot be reproduced by DFT even if SOC is taken into account. The latter split-band behavior at the saddle point cannot be attributed to structural modulations and cannot be clearly assigned to spin effects; therefore, it remains an open question distinguishing Ge from other similar systems as for example Sn-Ag (111) surface alloy.

ACKNOWLEDGMENTS

The authors acknowledge financial support from the FP7/Future and Emerging Technologies (FET) "2D-NANOLATTICES" Grant No. 270749 of the European Commission. The calculations used resources of the HellasGrid and EGEE computing infrastructure.

*Corresponding author: dimoulas@ims.demokritos.gr

[1] Y. A. Bychkov and E. I. Rashba, JETP Lett. **39**, 78 (1984).

[2] C. R. Ast, J. Henk, A. Ernst, L. Moreschini, M. C. Falub, D. Pacile, P. Bruno, K. Kern, and M. Grioni, Phys. Rev. Lett. **98**, 186807 (2007).

[3] D. Pacile, C. R Ast, M. Papagno, C. Da Silva, L. Moreschini, M. Falub, A. P. Seitsonen, and M. Grioni, Phys. Rev. B **73**, 245429 (2006).

[4] L. Moreschini, A. Bendounan, I. Gierz, C. R. Ast, H. Mirhosseini, H. Höchst, K. Kern, J. Henk, A. Ernst, S. Ostanin, F. Reinert, and M. Grioni, Phys. Rev. B **79**, 075424 (2009).

[5]J. R. Osiecki and R. I. G. Uhrberg, Phys. Rev. B **87**, 075441 (2013).
[6]P. Vogt, P. De Padova, C. Quaresima, J. Avila, E. Frantzeskakis, M. C Asensio, A. Resta, B. Ealet, and G. LeLay, Phys. Rev. Lett. **108**, 155501 (2012).
[7]D. Kaltsas, L. Tsetseris, and A. Dimoulas, J. Phys.: Condens. Matter **24**, 442001 (2012).
[8]S. Cahangirov, M. Topsakal, E. Aktürk, H. Şahin, and S. Ciraci, Phys. Rev. Lett. **102**, 236804 (2009).
[9]H. Oughaddou, S. Sawaya, J. Goniakowski, B. Aufray, G. Le Lay, J. M. Gay, G. Treglia, J. P. Biberian, N. Barrett, C. Guillot, A. Mayne, and G. Dujardin, Phys. Rev. B **62**, 16653 (2000).
[10]Y. Ohtsubo, S. Hatta, N. Kawai, A. Mori, Y. Takeichi, K. Yaji, H. Okuyama, and T. Aruga, Phys. Rev. B **86**, 165325 (2012).
[11]See Supplemental Material at http://link.aps.org/supplemental/10.1103/PhysRevB.88.075403 for details on the electronic band mapping of clean Ag(111) and the calculated band structure dependence on the Ge relaxation height.
[12]R. Courths, M. Lau, T. Scheunemann, H. Gollisch, and R. Feder, Phys. Rev. B **63**, 195110 (2001).
[13]G. Kresse and D. Joubert, Phys. Rev. B **59**, 1758 (1999).
[14]P. E. Blöchl, Phys. Rev. B **50**, 17953 (1994).
[15]J. P. Perdew, J. A. Chevary, S. H. Vosko, K. A. Jackson, M. R. Pederson, D. J. Singh, and C. Fiolhais, Phys. Rev. B **46**, 6671 (1992).
[16]K. He, T. Hirahara, T. Okuda, S. Hasegawa, A. Kakizaki, and I. Matsuda, Phys. Rev. Lett. **101**, 107604 (2008).
[17]G. Bian, L. Zhang, Y. Liu, T. Miller, and T.-C. Chiang, Phys. Rev. Lett. **108**, 186403 (2012).
[18]I. Gierz, B. Stadtmüller, J. Vuorinen, M. Lindroos, F. Meier, J. H. Dil, K. Kern, and C. R. Ast, Phys. Rev. B **81**, 245430 (2010).
[19]C. R. Ast, D. Pacilé, L. Moreschini, M. C. Falub, M. Papagno, K. Kern, M. Grioni, J. Henk, A. Ernst, S. Ostanin, and P. Bruno, Phys. Rev. B **77**, 081407(R) (2008).
[20]K. Sakamoto, H. Kakuta, K. Sugawara, K. Miyamoto, A. Kimura, T. Kuzumaki, N. Ueno, E. Annese, J. Fujii, A. Kodama, T. Shishidou, H. Namatame, M. Taniguchi, T. Sato, T. Takahashi, and T. Oguchi, Phys. Rev. Lett. **103**, 156801 (2009).
[21]E. Frantzeskakis, S. Pons, and M. Grioni, Phys. Rev. B **82**, 085440 (2010).
[22]C.-C. Liu, W. Feng, and Y. Yao, Phys. Rev. Lett. **107**, 076802 (2011).